Influence of heat treatments on microstructure and wear behavior of AISI H13 tool steel

Melika Ozer

Metallurgical and Materials Engineering, Faculty of Technology, Gazi University, 06560 Ankara, Turkey

Abstract

The influence of quenching and tempering heat treatments on the microstructure and wear behavior of AISI H13 tool steel was investigated. The austenitization was carried out at 1050 ℃. After austenitization, oil quenching, single tempering, and sequential double tempering treatments were carried out. The microstructure, hardness, and wear behavior of the samples were studied. Three different types of carbide particles, $M_{23}C_6$, MC, and M_7C_3, were determined in the microstructure. The sample, subjected to quenching, gave the highest hardness value. The double tempering process caused secondary hardening. After the abrasive wear tests, the greatest volume loss was observed in the as-received sample. With quenching and tempering heat treatments, the wear resistance of H13 steel increased significantly. The lowest volume loss among the applied heat treatments was obtained by quenching + double tempering.

K e y w o r d s: AISI H13, tool steel, wear, heat treatment, microstructure

1. Introduction

AISI H13 is a tool steel with superior properties such as excellent toughness, high wear resistance, hardenability, and high thermal shock resistance [1–4]. These superior properties and easy availability have made H13 steel popular among H-series hot work tool steels [4, 5]. It is widely preferred in casting, extrusion, forging, and rolling [6, 7].

The heat treatment process significantly affects the mechanical properties of the steel. Therefore, modifying the microstructure by optimizing the heat treatment steps is an effective way to increase the mechanical properties of H13 steel. Recent research has shown that different heat treatments can be applied to H13. However, quenching + tempering heat treatment cycles are conventionally applied to H13. After conventional quenching + tempering, the microstructure of H13 consists of tempered martensite, retained austenite, and carbide particles [3, 7]. Due to the C, Cr, Mo, and V content, there are $M_{23}C_6$, M_7C_3, M_2C, M_6C, and MC types of carbides in the microstructure of H13 [8–11].

AISI H13 steel is generally preferred in die manu-facturing. When the application areas of H13 steel are examined, there is intense friction between the product and/or semi-product with the die surfaces. The die surface/workpiece interaction causes abrasive wear on the die surfaces. Although the mechanical properties of H13 steel have been developed with various heat treatment optimizations, wear of the die surfaces is one of the main failure modes, significantly reducing the working life of the die [12–14].

Studies on the wear behavior of H13 are generally related to oxidative-type wear that occurs at high temperatures [14]. However, H13 is also widely used in forming processes at room temperature because of its high mechanical features. The morphology of the martensite phase, the size and distribution of the carbides, and the secondary carbides precipitated from the martensite significantly affect the performance of H13 steel at room temperature. Secondary carbides are considered the key strengthening step owing to their fine particle size and homogeneous distribution [15]. Therefore, in this study, the effects of heat treatments applied to H13 steel on martensite phase morphology, size and distribution of carbides, and thus hardness and wear resistance were investigated.

*Corresponding author: e-mail address: mcerah@gazi.edu.tr

Table 1. Chemical composition of AISI H13 steel (wt.%)

		C	Si	Mn	P	S	Cr	Mo	V	Fe
AISI H13	Nominal target	0.37–0.43	0.90–1.20	0.30–0.50	max. 0.025	max. 0.005	4.80–5.50	1.20–1.50	0.90–1.10	Bal.
	Experimental	0.39	0.97	0,37	0.020	0.001	4.90	1.25	0.94	

Table 2. The specimens notations and experimental plan

Sample notation	Heat treatment	Austenitization and oil quenching	1. Tempering process	2. Tempering process
H	As-received	–	–	–
HQ	Conventional quenching	1050 °C, 30 min + oil quenching	–	–
HQ + T	Conventional quenching + single tempering	1050 °C, 30 min + oil quenching	530 °C 180 min	–
HQ + T + T	Conventional quenching + double tempering	1050 °C, 30 min + oil quenching	530 °C 180 min	530 °C 180 min

2. Materials and methods

Commercial AISI H13 tool steel was used as test material. The chemical composition of H13 steel is given in Table 1.

Conventional quenching and tempering heat treatments were applied to the H13. Table 2 illustrates the specimen notations and experimental plan, and the heat treatment scheme is given in Fig. 1.

For the quenching process, austenitization was performed at 1050 °C. The austenitization process was carried out in a tube furnace with an argon shield atmosphere. The heating rate was 25 °C min^{-1}, and it waited for 30 min at the austenitization temperature. After austenitization, oil quenching was applied to the samples. Then, single tempering was applied to one sample series, and double tempering was applied to another. Tempering processes were performed at a temperature of 530 °C and a waiting time of 180 min, and the cycle was completed with cooling in air.

After heat treatments, the samples were prepared following metallographic methods and etched in a 2 % nital (HNO$_3$) solution. Microstructures of the specimens were analyzed using Light Optical Microscope (LOM), Scanning Electron Microscope (SEM), and Field Emission-SEM (FESEM). Through the heat treatments, carbides formed in the microstructure were determined via X-ray Diffraction (XRD). Macro hardness measurements of the samples were carried
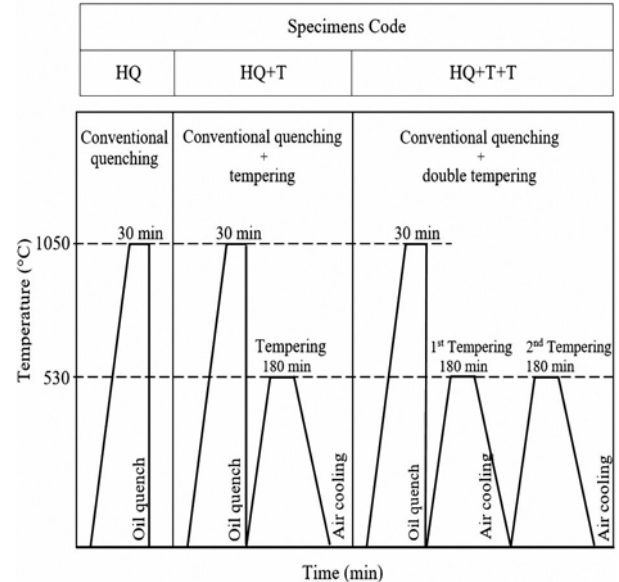

Fig. 1. The schematic illustration of heat treatment.

out with the Brinell hardness test in accordance with ASTM E 10-18. Abrasive wear tests were carried out with a dry test type pin-on-disc tribometer according to ASTM G99 standard. Samples for the tests were prepared in ⌀ 10 × 8 mm dimensions. The tests were carried out with 5, 10, and 15 N loads at different distances (500, 1000, and 1500 m) at 1 m s^{-1} speed.
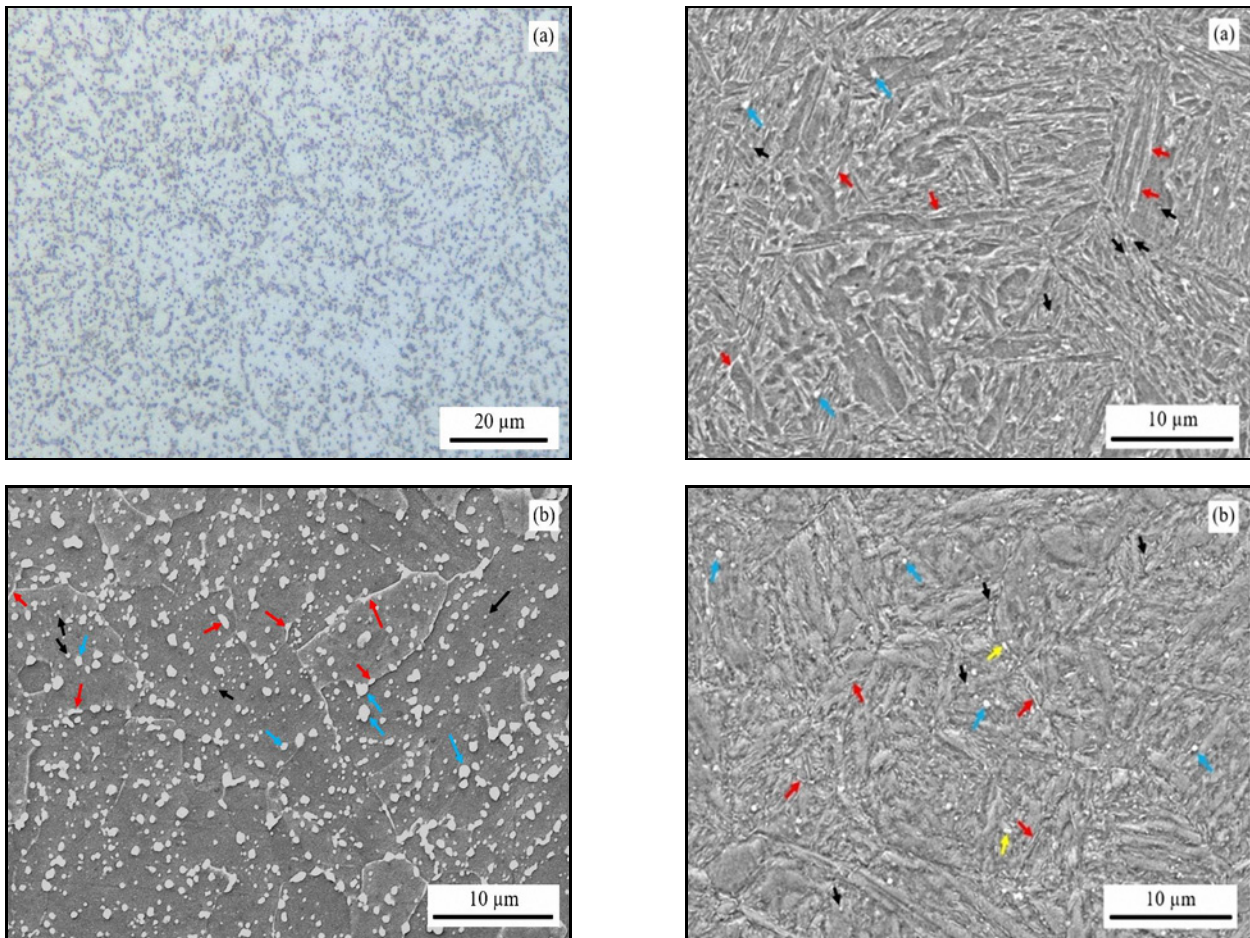
Fig. 2. Micrographs of AISI H13 as-received: (a) LOM and (b) SEM.

3. Results and discussion

3.1. Microstructure

LOM and SEM micrographs of the as-received sample are given in Fig. 2. The micrographs show that the microstructure consists of carbides precipitated in the ferrite matrix. It can be said that particles of different shapes and sizes (black dots in LOM images and white particles in SEM images) exhibit a homogeneous distribution throughout the structure (Figs. 2 and 3). In the literature, three different types of carbide with different shapes and sizes are mentioned [9, 15–17]. Type A (Figs. 2b and 3, red arrow) are strip-like carbides. They usually occur along grain boundaries. This type has a high aspect ratio. They are defined as chromium-rich $M_{23}C_6$-type carbides in the literature. Type B are carbides that exist in microstructure in the form of fine granules. Vanadium-(Figs. 2b and 3, black arrow) and molybdenum-rich (Figs. 2b and 3, blue arrow) are MC-type carbides. The V-rich carbides of the MC type have a finer size.
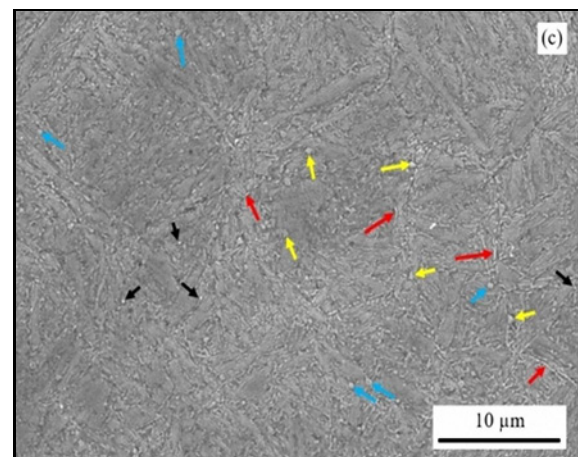

Fig. 3. SEM micrographs of samples: (a) HQ, (b) HQ + T, (c) HQ + T + T.

Type C (Fig. 3c, yellow arrow) are ellipsoid (and/or polygonized) coarse carbides. These are chromium-rich M_7C_3-type carbides.

SEM micrographs of HQ, HQ + T, and HQ + T + T samples are given in Fig. 3. Lath martensite was formed because AISI H13 contains 0.39 wt.% carbon. With the tempering process, the martensite
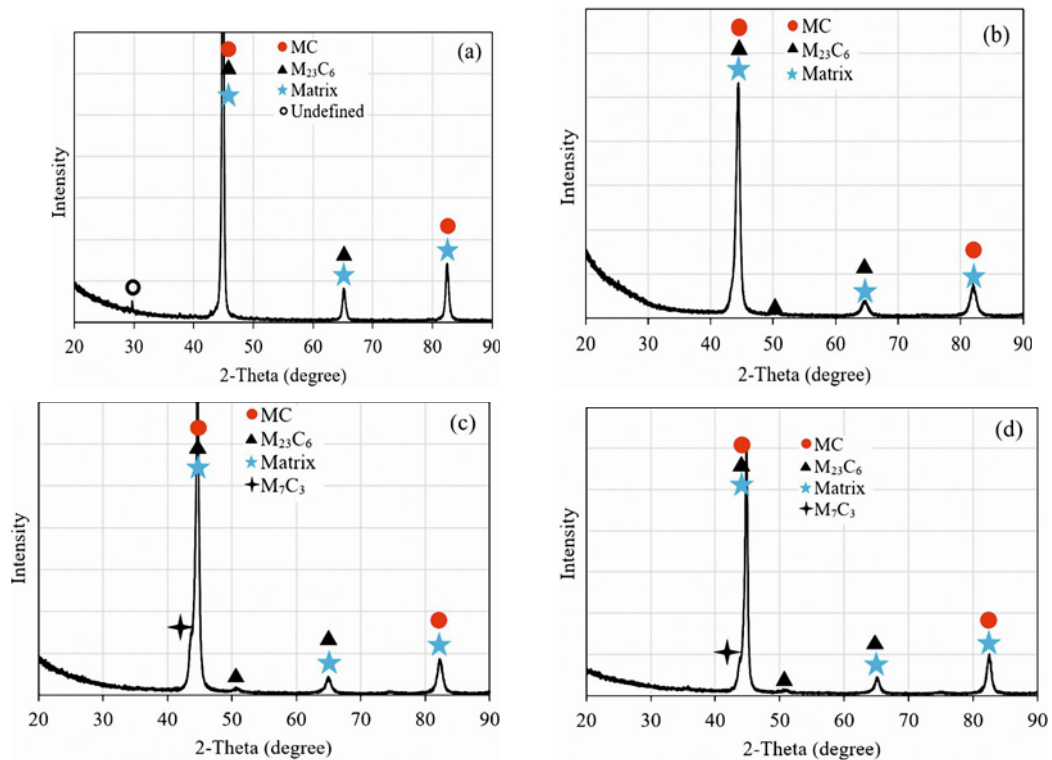
Fig. 4. The XRD patterns of samples: (a) As-received, (b) HQ, (c) HQ + T, and (d) HQ + T + T.

laths in the HQ + T and HQ + T + T samples expanded, and the shape sharpness of the martensite laths in the HQ sample decreased. It can be said that in tempered samples, carbides precipitate preferably at martensite lath boundaries due to low thermal activation energy. Figure 3 shows that carbides precipitate as granules (MC), ellipsoid (and/or polygonized) (M_7C_3) and strip-like ($M_{23}C_6$). With the effect of second tempering, the aspect ratio of strip-like carbides ($M_{23}C_6$) decreased. This is seen in the micrograph of the HQ + T + T sample given in Fig. 3c. Therefore, it can be said that carbide type and size are relevant to the number of tempering. In the literature, MC-type carbides in the microstructure of AISI H13 have been defined as primary carbides, while M_7C_3 and $M_{23}C_6$ type carbides have been defined as secondary carbides [7, 17].

The temperature, duration and number of tempering processes affect the type, shape, and size of the carbides that will form in the microstructure of H13 [15, 18–21]. In this study, the tempering temperature and time were fixed, and the number of tempering processes was changed. The effect of the heat treatment cycles applied to H13 steel on the carbide type was investigated with the XRD graph given in Fig. 4. When the XRD graphs given in Fig. 4 are examined in terms of the type of carbides, information confirming the microstructure pictures given in Fig. 3 has been obtained. Only the peaks of $M_{23}C_6$ and MC carbides were obtained in as-received and HQ samples.
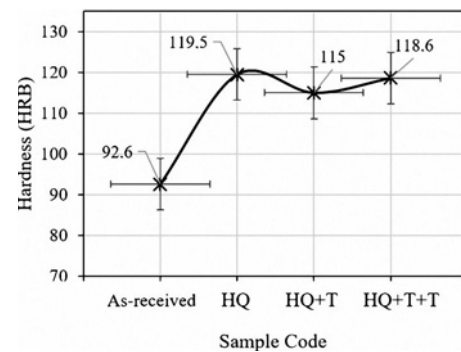

Fig. 5. Hardness graph of samples.

In HQ + T and HQ + T + T samples, in addition to $M_{23}C_6$ and MC carbide peaks, peaks belonging to M_7C_3 carbides were also obtained. In addition, larger peaks were obtained in the tempered samples compared to the HQ sample. This shows that after the tempering process, the carbide variety and volume ratio of the carbide particles increased in the samples. The type, volume ratio, size, and shape of the carbides in the microstructure significantly affect the mechanical properties of the material, like hardness and wear resistance.

3.2. Hardness

The macrohardness values of the samples are given in Fig. 5. With the quenching process, a considerable
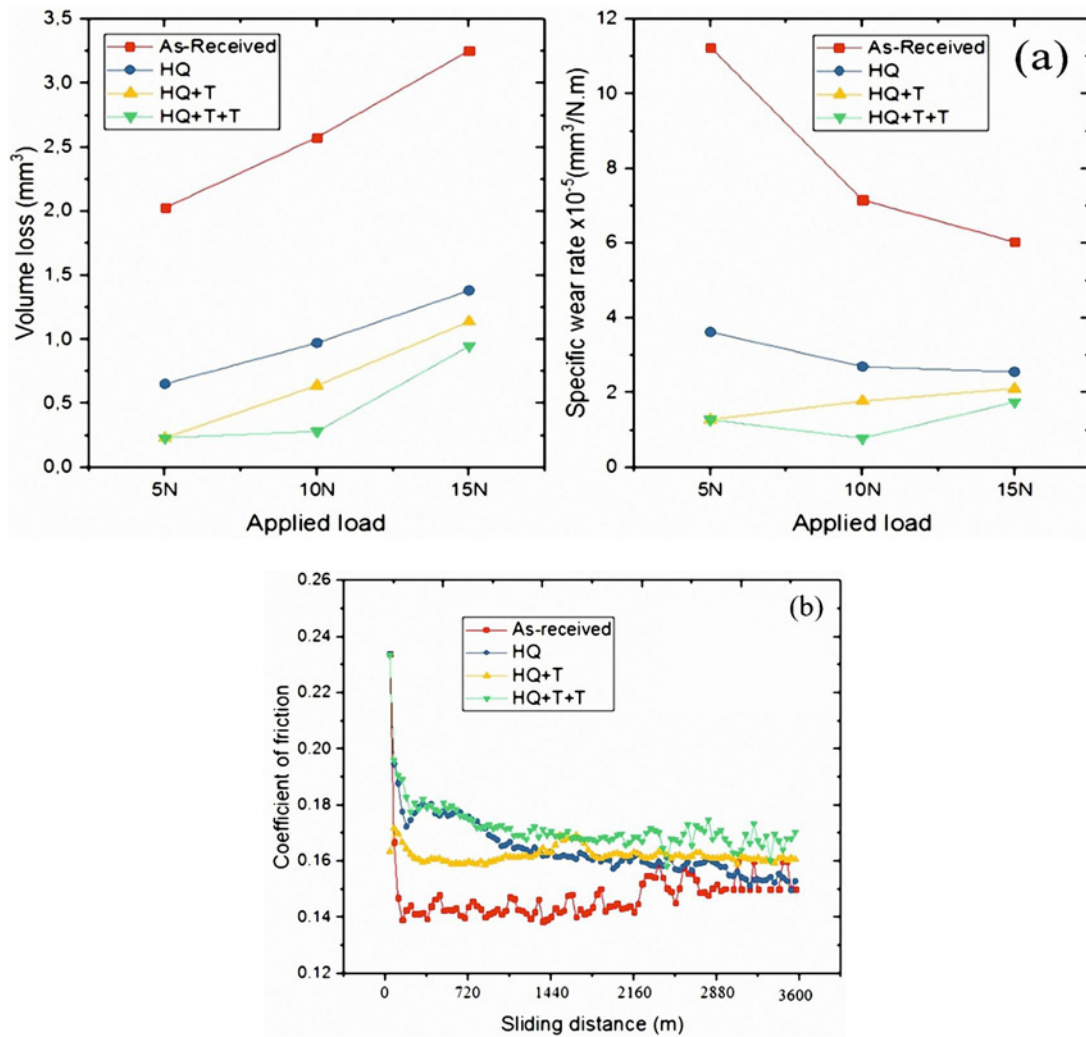
Fig. 6. (a) Volume loss and SWR graph and (b) CoF graph.

increase in hardness was observed compared to the as-received sample. The highest hardness value was determined in the HQ sample with 119.5 HRB.

With the single annealing heat treatment applied after the quenching process, a 4.5 HRB decrease was detected in the hardness values of the samples. A significant hardness decrease can be expected by transforming the martensite phase into tempered martensite by tempering [4]. However, the formation of M_7C_3 type carbides in addition to the existing carbides in the microstructure with the tempering process and the presence of more homogeneously dispersed complex carbides with the effect of tempering limited the decrease in hardness to 4.5 HRB. Moreover, the double tempering process caused secondary hardening. The smaller size and more homogeneous distribution of the carbides precipitated in the microstructure can be the reason for the secondary hardening that occurs with the second tempering. Prudente et al. [20] stated that the homogeneous and fine distribution of carbides in alloy steels causes secondary hardening.

3.3. Wear characteristics of heat-treated AISI H13 steel

The average volume loss and specific wear rates (SWR) of samples were determined and are presented graphically in Fig. 6a as a function of applied load for specimens with different heat-treated H13 and as-received. As expected, the volume loss increased with the increase of applied load in all samples. The greatest volume loss was observed in the as-received sample under all wear conditions. The wear resistance of H13 steel increased significantly with HQ, HQ + T, and HQ + T + T heat treatments. M_7C_3-type carbide particles caused HQ + T and HQ + T + T specimens to exhibit better tribological properties in wear tests. In the literature, it has been stated that the M_7C_3 type carbide particles that appear in the microstructure of the steel by tempering have a favorable efficacy on wear resistance [18, 20]. The lowest volume loss in the samples was obtained with the HQ + T + T process. The presence of secondary carbides in the HQ + T +
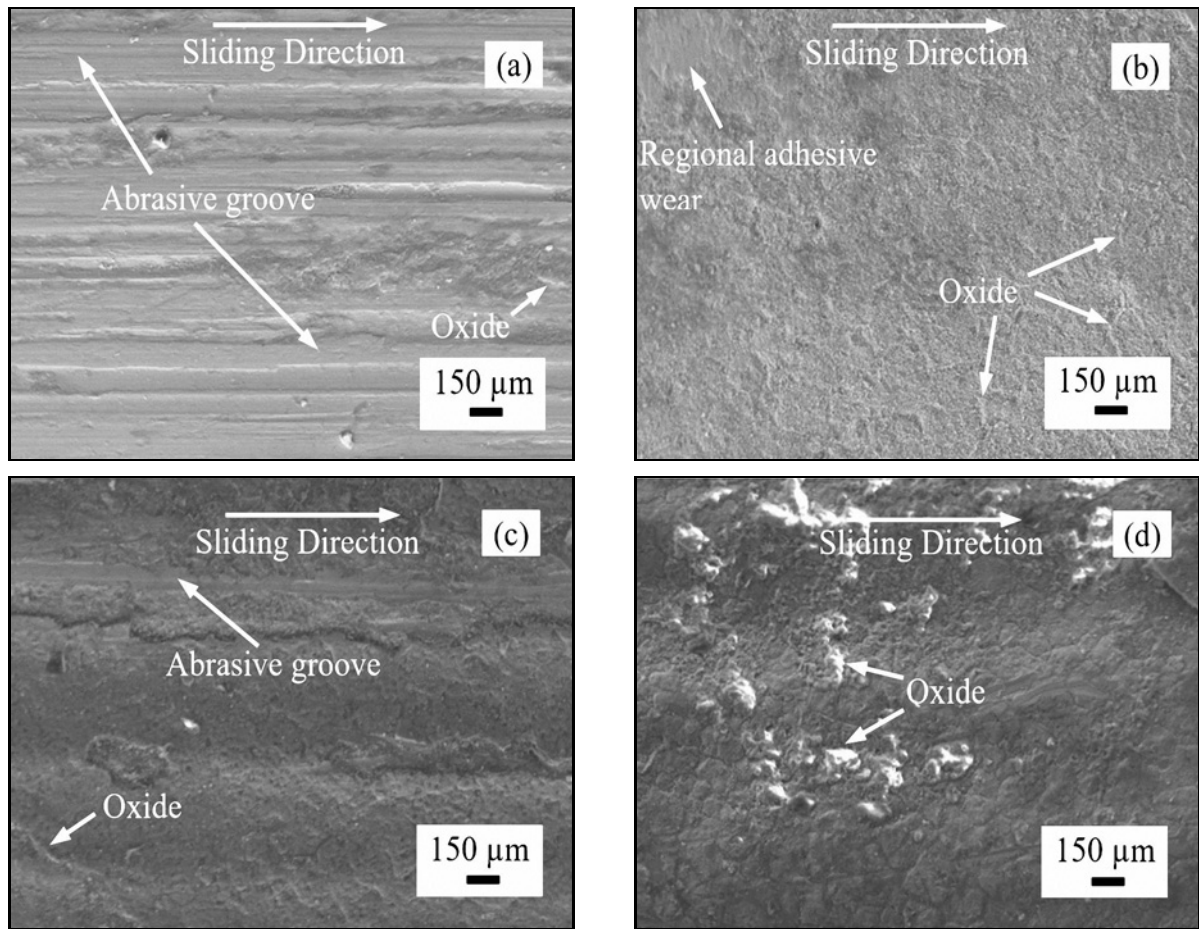
Fig. 7. Worn surface FESEM micrographs: (a) as-received, (b) HQ, (c) HQ + T, and (d) HQ + T + T.

T sample, the decrease in the carbides in the aspect ratio, and homogeneous and fine distribution improved the tribological properties of the sample together with secondary hardening. SWRs depend on mass, density, load, and sliding distance. SWR accurately describes the wear behavior, especially for metals, alloys, and composites [22–24]. The lowest SWR in all experimental parameters was obtained in the HQ + T + T sample under a 10 N load. It was observed that the SWR value decreased significantly with the increased applied load in the as-received and HQ specimens. This result shows that for as-received and HQ samples, the wear does not increase at the same rate as the applied load increases. Other results are similar to volume loss data. As a result, HQ + T + T heat treatment was determined to be the most suitable heat treatment for H13 in tribological systems.

Another important parameter for characterizing the wear behavior is the friction coefficient. The coefficient of friction (CoF) provides significant information about the tribological behavior of the sample [25]. The CoF values obtained during the wear tests under 15 N load are given in Fig. 6b. Since similar graphs were created for other loads, CoF values at the

Table 3. Average CoF values of heat-treated H13

Sample	As-received	HQ	HQ + T	HQ + T + T
CoF	0.15	0.16	0.16	0.17

highest load value were used to avoid confusion. It is seen that the CoF values are high at the beginning of the test and then follow a smooth line. Although the lowest CoF value was determined in the as-received sample, it is seen that there is no significant difference between it and the other samples. The average CoF values given in Table 3 also confirm this. As a result, it was determined that the applied heat treatments did not significantly affect the CoF of the H13 tool steel.

3.4. Worn surface SEM and EDS analysis

Worn surface FESEM images of the samples are given in Fig. 7 to characterize the wear conditions and surface deformation effects. Figure 7a shows the worn surface image of the as-received sample. Abrasive grooves formed by abrasion are located on the
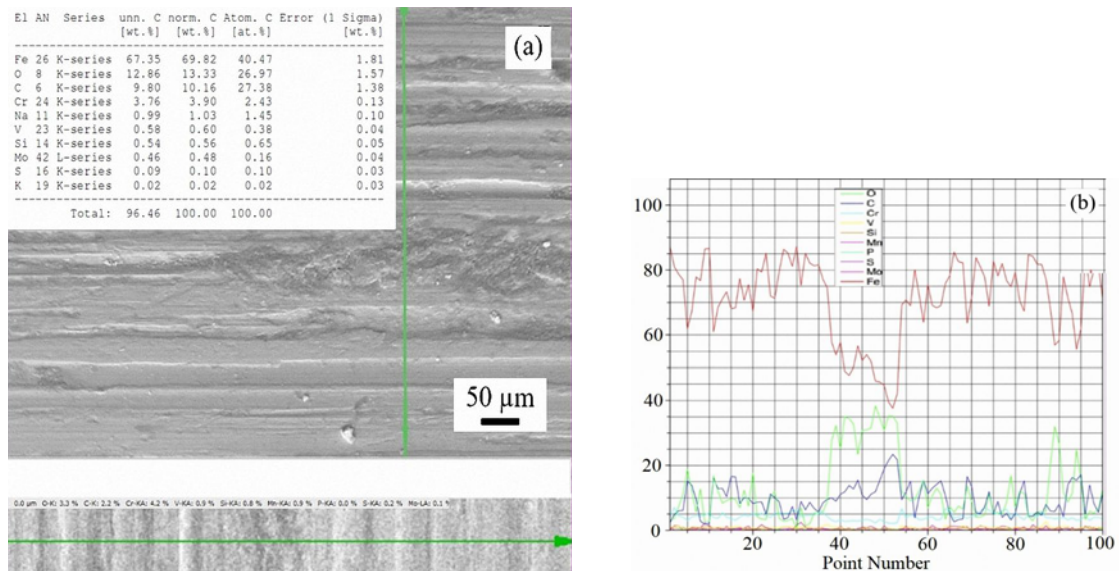
El AN Series	unn. C [wt.%]	norm. C [wt.%]	Atom. C [at.%]	Error (1 Sigma) [wt.%]
Fe 26 K-series	67.35	69.82	40.47	1.81
O 8 K-series	12.86	13.33	26.97	1.57
C 6 K-series	9.80	10.16	27.38	1.38
Cr 24 K-series	3.76	3.90	2.43	0.13
Na 11 K-series	0.99	1.03	1.45	0.10
V 23 K-series	0.58	0.60	0.38	0.04
Si 14 K-series	0.54	0.56	0.65	0.05
Mo 42 L-series	0.46	0.48	0.16	0.04
S 16 K-series	0.09	0.10	0.10	0.03
K 19 K-series	0.02	0.02	0.02	0.03
Total:	96.46	100.00	100.00	

Fig. 8. As-received sample: (a) FESEM micrographs and element distribution spectrometry and (b) linear element distribution graph.

El AN Series	unn. C [wt.%]	norm. C [wt.%]	Atom. C [at.%]	Error (1 Sigma) [wt.%]
Fe 26 K-series	51.78	53.67	27.29	1.41
O 8 K-series	18.33	18.99	33.71	2.36
C 6 K-series	12.61	13.07	30.90	1.94
Cr 24 K-series	6.36	6.60	3.60	0.20
Ni 28 K-series	3.51	3.63	1.76	0.14
V 23 K-series	1.12	1.16	0.65	0.06
Mo 42 L-series	0.95	0.98	0.29	0.07
Si 14 K-series	0.95	0.98	0.99	0.07
Al 13 K-series	0.44	0.45	0.48	0.05
Mn 25 K-series	0.22	0.23	0.12	0.04
S 16 K-series	0.19	0.19	0.17	0.03
P 15 K-series	0.04	0.04	0.04	0.03
Total:	96.49	100.00	100.00	
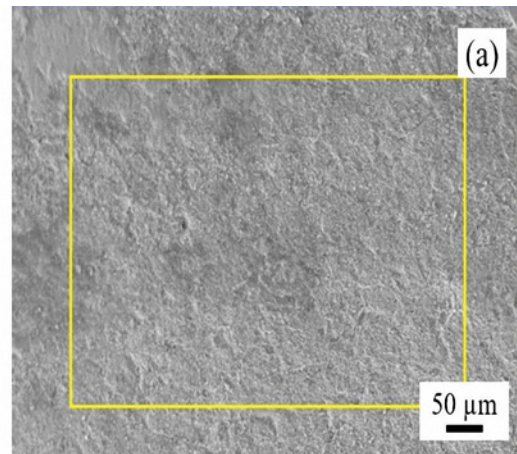
| El AN Series	unn. C [wt.%]	norm. C [wt.%]	Atom. C [at.%]	Error (1 Sigma) [wt.%]
Fe 26 K-series	50.98	51.67	22.89	1.38
O 8 K-series	26.51	26.88	41.55	3.07
C 6 K-series	15.28	15.48	31.89	2.01
Cr 24 K-series	2.27	2.30	1.09	0.09
Ni 28 K-series	1.34	1.36	0.57	0.07
Na 11 K-series	1.07	1.08	1.16	0.10
Si 14 K-series	0.51	0.52	0.46	0.05
V 23 K-series	0.34	0.34	0.17	0.04
Mn 25 K-series	0.18	0.19	0.08	0.03
S 16 K-series	0.14	0.14	0.11	0.03
P 15 K-series	0.04	0.04	0.03	0.03
Mo 42 L-series	0.00	0.00	0.00	0.00
Total:	98.65	100.00	100.00	
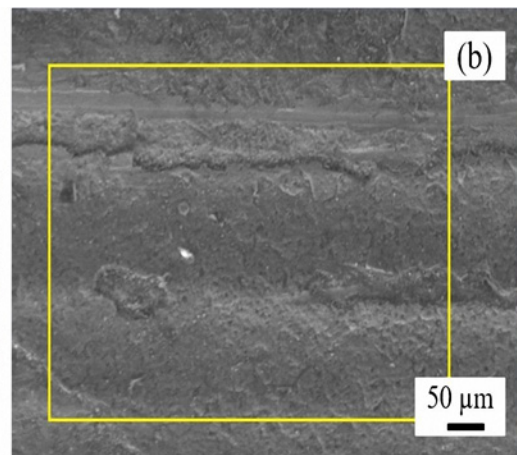
Fig. 9. The worn surface FESEM image and regional EDS analysis data: (a) HQ sample and (b) HQ + T sample.

surface. The low hardness and high ductility of the as-received sample caused plastic deformation on the surface. Numerous deep abrasive grooves have formed due to plastic deformation on the surface. Figure 7b
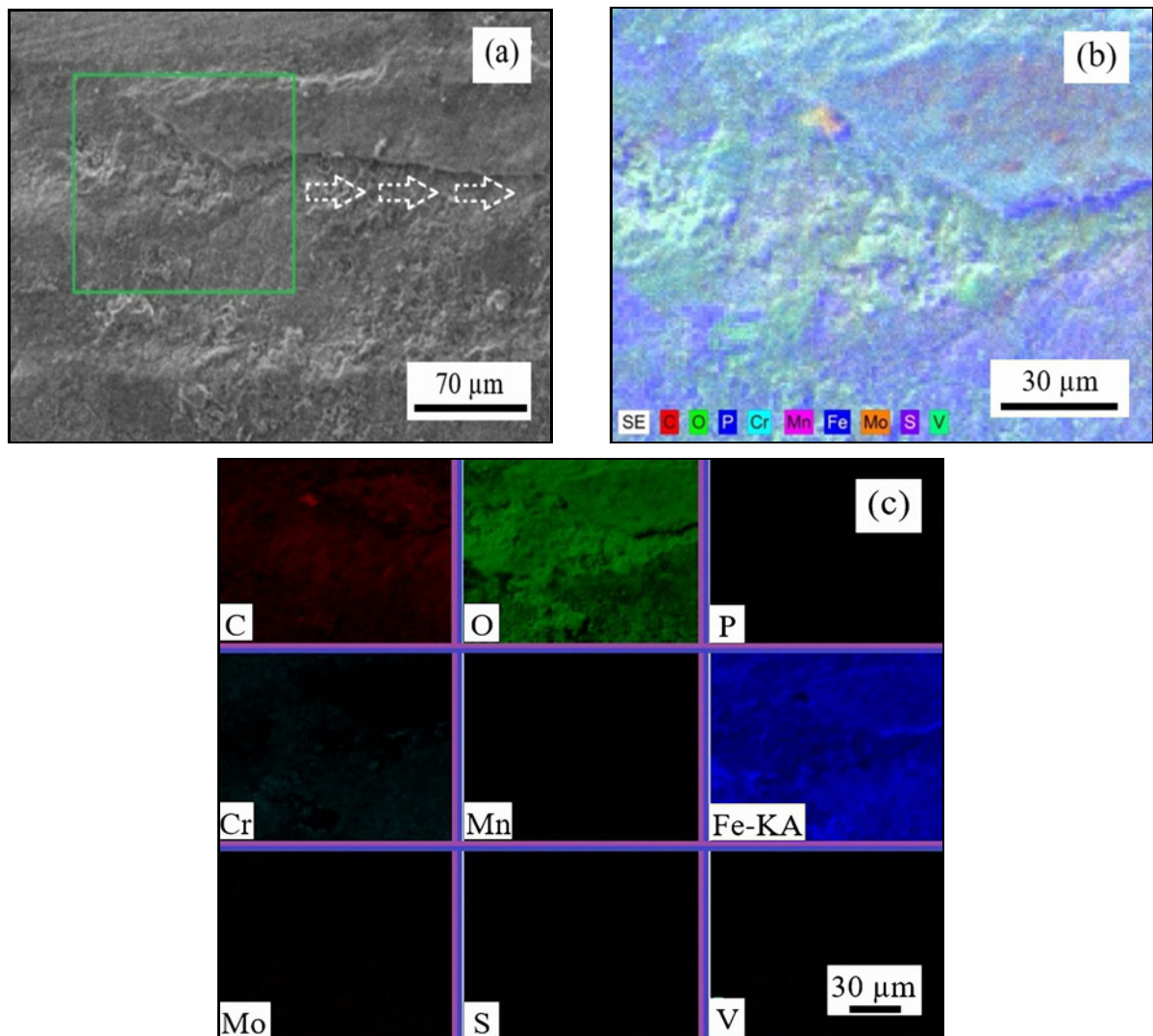
Fig. 10. HQ + T + T sample: (a) FESEM micrographs, (b) overall MAP analysis, and (c) elemental MAP analyses.

shows the worn surface of the HQ sample. The quenching treatment significantly increased the hardness and decreased the ductility. Therefore, no obvious wear grooves were observed on the wear surface. Local adhesive wear was observed with a smooth surface. In Fig. 7c, the wear surface of the HQ + T sample is given. With the tempering process, the hardness of the HQ + T specimen decreased, and its ductility increased. Therefore, plastic deformation and abrasive grooves at low penetration depth were observed on the wear surface. Figure 7d shows the wear surface FESEM micrograph of the HQ + T + T sample. No obvious wear grooves were observed due to secondary hardening by double tempering. In the wear tests of all samples, the heat generated at the interface caused a small number of oxide particles.

Figure 8 shows the EDS results of the as-received sample, the worn surface FESEM image, and the linear element distribution graph of the line analysis. It was determined that the most abundant elements on

the surface in wt.% were Fe, C, and O. O element has shown its existence due to oxides formed on the open surface by abrasion. The C content of the H13 sample was 0.39 wt.%. The presence of 1.38 wt.% C was determined on the sample surface. It is thought that C is transferred from the wear disc surface to the sample surface by the effect of friction. In the studies, the presence of O and C elements on the wear surface has been mentioned. In particular, it was emphasized that the O element directly affects the wear behavior with the oxide layers formed on the surface [26–28].

The worn surface FESEM image for the HQ sample and the regional EDS analysis data are given in Fig. 9a. Elements such as Fe, Cr, Mo, V, Si, and Mn, which should be included in the structure, and the O content due to the oxides formed on the surface were determined. The secondary phases formed by elements such as Cr, Mo, and V, determined on the sample surface, positively affect the wear behavior. The worn surface FESEM image of the HQ + T sample and

the regional EDS analysis data are given in Fig. 9b. When Fig. 9b is examined, the abrasive grooves and deformation effects that occur after wear are clearly seen. From the EDS data, the elements that should be included in the structure and the presence of element O due to the oxides formed on the surface were determined.

Figure 10 shows the worn surface micrograph and MAP images of the HQ + T + T sample. It can be said that Fe, C, O, and Cr elements indicate homogeneous distribution on the sample surface. Wear data and MAP analyses were helpful in the evaluation. With the applied second tempering process, the formation and homogeneous distribution of M_7C_3 and $M_{23}C_6$ type Cr-containing carbide precipitates in the microstructure were determined. These homogeneously dispersed carbides contributed to the improvement of wear properties by playing an active role [29].

4. Conclusions

The main conclusions of this study are summarized below:

– $M_{23}C_6$, MC, and M_7C_3 carbide particles were determined in the microstructure of AISI H13 steel. It was determined that the tempering process increased the carbides diversity and the volume ratio of carbides.

– It was determined that carbides in tempered samples precipitated preferentially at martensite lath boundaries.

– The quenched sample gave the highest hardness value. A slight decrease in the hardness values of the samples was determined with the single tempering process applied after the quenching process. The double tempering process caused secondary hardening.

– After the abrasive wear tests, the greatest volume loss was observed in the as-received sample. With the quenching and tempering processes, the wear resistance of H13 steel increased significantly.

– Numerous deep abrasive grooves were detected on the surface of the as-received sample. No wear grooves were observed in the quenched sample. Abrasive grooves with less penetration depth were observed on the surface of the sample that was quenched + tempered. No wear grooves were observed due to secondary hardening in the quenched + double tempered heat-treated sample.

References

[1] J. Y. Li, Y. L. Chen, J. H. Huo, Mechanism of improvement on strength and toughness of H13 die steel by nitrogen, Mat. Sci. Eng. A 640 (2015) 16–23. https://doi.org/10.1016/j.msea.2015.05.006

[2] A. Çiçek, F. Kara, T. Kivak, E. Ekici, Evaluation of machinability of hardened and cryo-treated AISI H13 hot work tool steel with ceramic inserts, Int. J. Refract. Met. H. 41 (2013) 461–469. https://doi.org/10.1016/j.ijrmhm.2013.06.004

[3] M. Koneshlou, K. M. Asl, F. Khomamizadeh, Effect of cryogenic treatment on microstructure, mechanical and wear behaviors of AISI H13 hot work tool steel, Cryogenics 51 (2011) 55–61. https://doi.org/10.1016/j.cryogenics.2010.11.001

[4] M. Özer, The effect of deep cryogenic processing and tempering heat treatment of AISI H13 tool steel on microstructure, hardness and impact energy (in Turkish), GU J. Sci. C 7 (2019) 688–699. https://doi.org/10.29109/gujsc.603355

[5] M. Perez, F. J. Belzunce, The effect of deep cryogenic treatments on the mechanical properties of an AISI H13 steel, Mat. Sci. Eng. A 624 (2015) 32–40. https://doi.org/10.1016/j.msea.2014.11.051

[6] T. Shinde, Failure analysis of cryogenically treated H13 specimen in rotating bending fatigue, Eng. Fail. Anal. 113 (2020) 104535. https://doi.org/10.1016/j.engfailanal.2020.104535

[7] T. Shinde, N. B. Dhokey, Influence of carbide density on surface roughness and quasi-stable wear behaviour of H13 die steel, Surface Eng. 33 (2017) 944–952. https://doi.org/10.1080/02670844.2017.1312739

[8] M.-T. Mao, H.-J. Guo, F. Wang, X.-L. Sun, Chemical composition and structural identification of primary carbides in as-cast H13 steel, Int. J. Min. Met. Mater. 26 (2019) 839–848. https://doi.org/10.1007/s12613-019-1796-7

[9] T. Shinde, Influence of carbide particle size on the wear performance of cryogenically treated H13 die steel, Surface Eng. 37 (2021) 1206–1214. https://doi.org/10.1080/02670844.2019.1701858

[10] C. P. Tabrett, I. R. Sare, M. R. Ghomashchi, Microstructure-property relationships in high chromium white iron alloys, Int. Mater. Rev. 41 (1996) 59–82. https://doi.org/10.1179/imr.1996.41.2.59

[11] A. Inoue, Y. Harakawa, M. Oguchi, T. Masumoto, Metastable MC phase in melt-quenched Fe-C-V and Fe-C-V-(Cr or Mo) alloys – mechanical properties and powder-forming tendency by comminution, J. Mater. Sci. 21 (1986) 1310–1320. https://doi.org/10.1007/BF00553269

[12] Z. Cao, S.-Q. Wang, K.-Z. Huang, B. Zhang, G.-H. Wen, Q.-Y. Zhang, L. Wang, Effect of artificial tribological layer on sliding wear behavior of H13 steel, J. Iron Steel Res. Int. 24 (2017) 943–949. https://doi.org/10.1016/S1006-706X(17)30137-1

[13] H. Chen, Y. Lu, Y. Sun, Y. Wei, X. Wang, D. Liu, Coarse TiC particles reinforced H13 steel matrix composites produced by laser cladding, Surf. Coat. Tech. 395 (2020) 125867. https://doi.org/10.1016/j.surfcoat.2020.125867

[14] Y. Zhou, W. Jiang, Effect of sliding speed on elevated-temperature wear behavior of AISI H13 steel, J. Iron Steel Res. Int. 28 (2021) 1180–1189. https://doi.org/10.1007/s42243-021-00644-9

[15] A. Ning, W. Mao, X. Chen, H. Guo, J. Guo, Precipitation behavior of carbides in H13 hot work die steel and its strengthening during tempering, Metals 7 (2017) 70. https://doi.org/10.3390/met7030070

[16] R. Chen, Z. Wang, L. Qi, L. Zhong, R. Guan, J. He, X. Hu, The carbides, tensile properties, and work-hardening behavior of annealed H13 die steels with

varied yttrium contents, Mat. Sci. Eng. A 806 (2021) 140856. https://doi.org/10.1016/j.msea.2021.140856

[17] H. Wang, J. Li, C-B. Shi, J. Li, B. He, Evolution of carbides in H3 steel in heat treatment process, Mater. Trans. 58 (2017) 152–156.
https://doi.org/10.2320/matertrans.M2016268

[18] J. Wang, Z. Xu, X. Lu, Effect of the quenching and tempering temperatures on the microstructure and mechanical properties of H13 steel, J. Mater. Eng. Perform. 29 (2020) 1849–1859.
https://doi.org/10.1007/s11665-020-04686-0

[19] S. Yue, R. Gao, L. Li, H. Guo, Influence of tempering time on the behavior of large carbides' coarsening in AISI H13 steel, Metals 9 (2019) 1283.
https://doi.org/10.3390/met9121283

[20] W. R. Prudente, J. F. C. Lins, R. Siqueira, P. S. N. Mendes, R. E. Pereira, Microstructural evolution under tempering heat treatment in AISI H13 hot-work tool steel, Int. J. of Engineering Research and Application 7 (2017) 67–71.

[21] Z.-X. Jia, Y.-W. Liu, J.-Q. Li, L.-J. Liu, L.-H. Li, Crack growth behavior at thermal fatigue of H13 tool steel processed by laser surface melting, Int. J. Fatigue 78 (2015) 61–71.
https://doi.org/10.1016/j.ijfatigue.2015.04.005

[22] A. Mavi, Y. Kaplan, S. Aksoz, Effects of aging and deep cryogenic treatment on wear behavior of Al7075 alloy, J. Tribol. 143 (2021) 121702.
https://doi.org/10.1115/1.4052481

[23] S. Aksöz, S. Kaner, Y. Kaplan, Tribological and aging behavior of hybrid Al 7075 composite reinforced with B$_4$C, SiC, and TiB$_2$, Sci. Sinter. 53 (2021) 311–321.
https://doi.org/10.2298/SOS2103311A

[24] O. Altuntaş, A. Güral, Designing spherical cementite in bainitic matrix (SCBM) microstructures in high carbon powder metal steels to improve dry sliding wear resistance, Materials Letters 249 (2019) 185–188.
https://doi.org/10.1016/j.matlet.2019.04.095

[25] Y. Kaplan, S. Aksöz, H. Ada, E. İnce, S. Özsoy, The effect of aging processes on tribo-metallurgy properties of Al based ternary alloys product by P/M technique, Sci. Sinter. 52 (2020) 445–456.
https://doi.org/10.2298/SOS2004445K

[26] Y. Kaplan, A. Yıldırım, S. Aksöz, The effect of oxidation process after nitrocarburization on tribological properties of AISI 4140 steel (in Turkish), Journal of Polytechnic 23 (2020) 1357–1362.
https://doi.org/10.2339/politeknik.585031

[27] İ. Şimşek, M. Yıldırım, D. Özyürek, D. Şimşek, Investigation of wear behaviors of SiO$_2$ reinforced aluminium composites produced by pressureless infiltration method (in Turkish), Journal of Polytechnic 22 (2019) 81–85.
https://doi.org/10.2339/politeknik.389637

[28] N. Saka, A. M. Eleiche, N. P. Suh, Wear of metals at high sliding speeds, Wear 44 (1977) 109–125.
https://doi.org/10.1016/0043-1648(77)90089-8

[29] S. Aksöz, Wear behavior of hot forged NiTi parts produced by PM Technique, T. Indian I. Metals 72 (2019) 1949–1957.
https://doi.org/10.1007/s12666-019-01671-7